





Stabilization method with the relativistic configuration-interaction calculation applied to two-electron resonances

P. Amaro ¹, J. P. Santos ^{1,*}, S. Bhattacharyya ², T. K. Mukherjee,³ and J. K. Saha ^{4,†}

¹Laboratory for Instrumentation, Biomedical Engineering and Radiation Physics (LIBPhys-UNL), Department of Physics, NOVA School of Science and Technology, FCT, NOVA University Lisbon, 2829-516 Caparica, Portugal

²Department of Physics, Acharya Prafulla Chandra College, New Barrackpore, Kolkata 700131, India

³Department of Physics, Narula Institute of Technology, Agarpara, Kolkata 700109, India

⁴Department of Physics, Aliah University, IIA/27, Newtown, Kolkata 700160, India



(Received 6 September 2020; revised 22 November 2020; accepted 17 December 2020; published 21 January 2021)

We applied a relativistic configuration-interaction (CI) framework to the stabilization method as an approach for obtaining the autoionization resonance structure of heliumlike ions. In this method, the ion is confined within an impenetrable spherical cavity, the size of which determines the radial space available for electron wave functions and electron-electron interactions. By varying the size of the cavity, one can obtain the autoionization resonance position and width. The applicability of this method is tested on the resonances of He atom while comparing with benchmark data available in the literature. The present method is further applied on the determination of the resonance structure of heliumlike uranium ion, where a relativistic framework is mandatory. In the strong-confinement region, the present method can be useful to simulate the properties of an atom or ion under extreme pressure. An exemplary application of the present method to determine the structure of ions embedded in dense plasma environment is briefly discussed.

DOI: [10.1103/PhysRevA.103.012811](https://doi.org/10.1103/PhysRevA.103.012811)

I. INTRODUCTION

Resonance states are formed in different types of scattering experiments and the nature of interaction with the continuum of the target quantifies the width (or lifetime) of a resonance state. Due to the advancement of experimental techniques and with the advent of free electron lasers, recent interest has been generated to study the resonances of multiply charged ions [1–5]. Different theoretical approaches, e.g., complex coordinate rotation method [6], Feshbach projection operator method, optical potential method, R -matrix method, etc. (see, e.g., Ref. [7] and references therein) have been proposed to understand the internal structure of resonances. All these techniques need either the complete form of the wave functions, the use of complex analytic continuation, or the asymptotic form of the wave functions. Hazi and co-workers [8,9] were the pioneers to introduce the stabilization method for analyzing resonance states arising from elastic scattering with a one-dimensional model barrier potential. After the trial of several variants of this method over more than two decades, finally Mandelshtam *et al.* [10] put forward an elegant method of calculating the width of resonance states from the spectral density of states (DOS) in the neighborhood of resonance position. The idea of this method [10] is to diagonalize the Hamiltonian of a quantum system with suitable square-integrable real wave functions within a box, and investigate the continuum, bound, and resonances (autoionizing)

states under variations of the box size. The continuum states of atomic systems are strongly modified by changes of the box size, while in contrast, the resonance states are hardly affected by the variation of box size, if the minimum size of the box is greater than the effective extent of the wave function, or the range of the Coulomb potential. For a bound state, the eigenvalue converges to a particular value with the increase of box size [11,12]. The idea of the box is, therefore, to span the radial space in order to distinguish the variations of these three different types of states. There are different adaptations on the variations of this box. The early workers [8,9,13] defined the box size as a constraint parameter, usually termed as *hard wall*, in a finite basis set method. Later, Ho [14] and Müller *et al.* [15] modified the idea of *hard wall* by the *soft wall*, which can be considered as an arbitrary real continuous scaling parameter in a finite basis set. This conjecture [15] proved to be a very successful one to predict parameters for a wide range of resonances of free, confined as well as field induced few-body systems, where Hylleraas type basis sets are used [4,16–27]. Accruing larger radial space through the variation of the scaling parameter is also computationally more convenient than expanding the basis by including high-lying configurations as the latter may introduce the problem of linear dependency for large basis. The stabilization method has further been extended to determine the atomic resonances near metal surfaces [28], resonances in molecules [29,30], core-excited shape resonances in clusters [31,32], as well to probe nuclear resonances [33].

In the present work, we propose a hybrid technique where the stabilization method has been adopted within the framework of relativistic configuration-interaction (CI) calculation.

*jps@fct.unl.pt

†jsaha84@gmail.com

A correlated two-electron atomic system where the radial space is truncated by an impenetrable spherical box is considered as a bench-test case. By confining a quantum mechanical system within a model impenetrable spherical cavity and imposing appropriate boundary conditions, the basis sets and the matrix elements can be made explicitly dependent on the radius of the sphere. The electron orbitals are obtained from a finite basis set of B-splines defined in this impenetrable box, thus making this a *hard wall* method. This method has a twofold advantage. First, when the size of the box is reasonably small, the effect of confinement modifies the energy levels of the “free” ion and various problems of spatial confinement, e.g., pressure ionization in plasma environment [34] can be probed. With the advent of modern high-speed computational resources and experimental techniques for controlling and confining atoms along with their applications in semiconductors and nanotechnology, this topic of confined systems continues to attract interest nowadays. Manifold applications of such confined quantum mechanical systems are available in literature, e.g., atoms encaged in endohedral fullerenes [35], semiconductor quantum dots [26,36–39], ion storage [40], warm dense plasmas [41], etc. Comprehensive reviews on this topic may be found in Refs. [42–44]. Secondly, ensuring the radius of the cavity large enough, one can employ the stabilization method [45] for determining the parameters of resonance states. To the best of our knowledge, none of the existing variants of the stabilization method has been applied under the relativistic framework for probing the resonances of highly charged ions or in many-body systems. Both aspects of this spatial confinement within the relativistic stabilization framework are developed and discussed here. In this “hard wall” approach the radius of the cavity in the relativistic CI method is spanned in order to locate positions and widths of resonances. To validate the method, the resulting positions and widths of low-lying resonances of He atom are compared with benchmark nonrelativistic calculations [46,47]. As an example, we consider the case with null total angular momentum. The relativistic stabilization method is further extended for the heliumlike uranium ion to determine the resonance parameters. This method can be exploited to determine the structural properties of highly charged ions under spatial confinement and application in the dense plasma environment is also briefly presented here. The details of the methodology are given in Sec. II followed by the discussion on the results in Sec. III. Final conclusions are given in Sec. IV.

II. THEORY

A. Configuration interaction

We followed the configuration-interaction method of Ref. [48], to solve the two-electron Dirac Hamiltonian,

$$\hat{H}(\mathbf{r}_1, \mathbf{r}_2) = \hat{h}_0(\mathbf{r}_1) + \hat{h}_0(\mathbf{r}_2) + V(\mathbf{r}_1, \mathbf{r}_2), \quad (1)$$

where $\hat{h}_0(\mathbf{r})$ is a single-electron Dirac Hamiltonian solved in a B-spline basis set (see Sec. II B) with the nuclear potential being corrected for a nuclear finite size. The two-electron wave function with total angular momentum J , and respective projection over z of M and parity Π , is defined as a linear combination of configuration-state functions (CSF) of these

single-electron solutions, given by

$$\begin{aligned} \Psi_{\Pi}^J &= \sum_{x \leq y} C_{xy}^n \Psi_{xy}^{\text{CSF}}(JM) \\ &= \frac{1}{\sqrt{2}} \sum_{x \leq y} \mu_{xy} C_{xy} \langle j_x m_x j_y m_y | JM \rangle \begin{vmatrix} \psi_x(1) & \psi_y(1) \\ \psi_x(2) & \psi_y(2) \end{vmatrix}. \end{aligned} \quad (2)$$

Here, $\Psi_{xy}^{\text{CSF}}(JM)$ represents the CSF of two spherically confined hydrogenic orbitals identified by x and y that involves the ground orbitals and excitations from the occupied to virtual orbitals. The term μ_{xy} is given by

$$\mu_{xy} = \begin{cases} 1/\sqrt{2} & \text{if } x = y \\ 1 & \text{if } x \neq y \end{cases}. \quad (3)$$

By inserting this two-electron wave function in the Dirac equation, the problem of obtaining the respective eigenvalues is equivalent to diagonalizing the following eigenvalue equation:

$$\sum_{x \leq y} [(\epsilon_v + \epsilon_w) \delta_{xv} \delta_{yw} + V_{vw,xy}] C_{xy} = E C_{vw}, \quad (4)$$

where ϵ_v and E represent the hydrogenic energy of an orbital v and the total energy, respectively. The matrix element $V_{vw,xy} = \langle \Phi_{vw}(JM) | V | \Phi_{xy}(JM) \rangle$ of the electron-electron Coulomb interaction is given by

$$\begin{aligned} V_{vw,xy} &= \mu_{vw} \mu_{xy} \sum_k (-1)^{J+k+j_w+j_x} \begin{Bmatrix} j_v & j_w & J \\ j_y & j_x & k \end{Bmatrix} T_k(vwxy) \\ &\quad + (-1)^{k+j_w+j_x} \begin{Bmatrix} j_v & j_w & J \\ j_x & j_y & k \end{Bmatrix} T_k(vwyx). \end{aligned} \quad (5)$$

The quantity $T_k(vwyx)$ contains the Coulomb interaction and is given by

$$T_k(vwyx) = (-1)^k \langle \kappa_v \| C^k \| \kappa_x \rangle \langle \kappa_w \| C^k \| \kappa_y \rangle R_k(vwyx), \quad (6)$$

where the reduced matrix element $\langle \kappa_v \| C^k \| \kappa_x \rangle$ evaluates to

$$\begin{aligned} \langle \kappa_v \| C^k \| \kappa_x \rangle &= (-1)^{j_v+1/2} \sqrt{[j_v, j_x]} \\ &\quad \times \begin{pmatrix} j_v & j_x & k \\ -\frac{1}{2} & \frac{1}{2} & 0 \end{pmatrix} \Pi(l_v + k + l_x), \end{aligned} \quad (7)$$

with $\Pi(l)$ being the parity term. The Slater integrals $R_k(vwxy)$, defined by

$$\begin{aligned} R_k(vwxy) &= \int_0^R dr_1 [P_v(r_1)P_x(r_1) + Q_v(r_1)Q_x(r_1)] v_k(w, y, r_1), \end{aligned} \quad (8)$$

contains the overlaps of the large $P(r)$ and small $Q(r)$ components of the hydrogenic orbitals,

$$\begin{aligned} v_k(w, y, r_1) &= \int_0^R dr_2 \frac{r_2^k}{r_2^{k+1}} [P_w(r_2)P_y(r_2) + Q_w(r_2)Q_y(r_2)]. \end{aligned} \quad (9)$$

Here, R is the radius of the cavity. Although we did not include Breit interaction in this calculation, as one shall see in Sec. II D, differences in energies with *state-of-the-art* calculations are of 0.2%–0.3% in heliumlike uranium. Therefore,

although Breit interaction is important for precise determination of the resonances and critical radius (see Sec. III) beyond this uncertainty, the inclusion of only Coulomb potential is (nevertheless) sufficient as *proof of principle* of the CI to the stabilization method.

We now describe the method of the finite basis set with B-splines for which we obtain the hydrogenic wave functions confined in a cavity.

B. Finite basis set with B-splines

In the finite basis set approach, the atomic or molecular system is enclosed in a finite cavity with a radius R . This leads to a discretization of the continua and, hence, to a representation of the entire Dirac spectrum in terms of the pseudostate basis functions. A (quasicomplete) finite set of these states are determined subsequently by making use of the variational Galerkin method [49]. In this method, the action S_κ is defined as

$$S_\kappa = \frac{1}{2} \int_0^R \{cP_{n\kappa}(r)O_-^\kappa Q_{n\kappa}(r) - cQ_{n\kappa}(r)O_+^\kappa P_{n\kappa}(r) + V(r)[P_{n\kappa}(r)^2 + Q_{n\kappa}(r)^2] - 2m_e c^2 Q_{n\kappa}(r)^2\} dr - \frac{1}{2} \epsilon \int_0^R [P_{n\kappa}(r)^2 + Q_{n\kappa}(r)^2] dr + S_\kappa^{\text{bond}}, \quad (10)$$

from which the Dirac equation states can be derived from the least action principle, $\delta S_\kappa = 0$. To shorten the expressions, we introduced here the operator $O_\pm^\kappa = \frac{d}{dr} \pm \frac{\kappa}{r}$.

The parameter ϵ is a Lagrange multiplier introduced to ensure the normalization constraint [Eq. (10)]. Here, the large, $P_{n\kappa}(r)$, and small, $Q_{n\kappa}(r)$, radial components of the electron wave functions can be written as a finite expansion,

$$P(r) = \sum_{i=1}^N p_i B_i(r), \quad Q(r) = \sum_{i=1}^N q_i B_i(r), \quad (11)$$

over the B-spline basis set $B_i(r)$ that are given in detail in Sec. II C. Moreover, in Eq. (11), the subscripts n and κ have been omitted from the functions $P_{n\kappa}(r)$ and $Q_{n\kappa}(r)$ for the sake of notation simplicity. The function S_κ^{Bond} in Eq. (10), given by

$$S_\kappa^{\text{Bond}} = \begin{cases} \frac{\epsilon}{4} [P^2(R) - Q^2(R)] + \frac{\epsilon}{2} P(0) [P(0) - Q(0)] & \text{for } \kappa < 0 \\ \frac{\epsilon}{4} [P^2(R) - Q^2(R)] + \frac{\epsilon}{2} P(0) [2cP(0) - Q(0)] & \text{for } \kappa > 0 \end{cases} \quad (12)$$

assures the boundary conditions $P(0) = 0$ and $P(R) = Q(R)$ known as the MIT-bag-model condition [50], was included to avoid the Klein's paradox, which arises when one attempts to confine a particle to a cavity, essentially by forcing the radial current crossing the boundary to vanish [51].

Inserting the radial components (11) into the least action principle (10) and evaluating the variation S_κ with respect to change of the expansion coefficients p_i and q_i , we obtain the matrix equation,

$$Av = \epsilon Bv, \quad (13)$$

where $v = (p_1, p_2, \dots, p_N, q_1, q_2, \dots, q_N)$. A and B are symmetric $2N \times 2N$ matrices given, respectively, by

$$A = \begin{bmatrix} (V) & c[(D) - (\frac{\kappa}{r})] \\ -c[(D) + (\frac{\kappa}{r})] & -2c^2(C) + (V) \end{bmatrix} + A^{\text{bond}}, \quad (14)$$

and

$$B = \begin{bmatrix} (C) & 0 \\ 0 & (C) \end{bmatrix}. \quad (15)$$

The matrix A^{bond} reflects the boundary conditions, and is defined by

$$A_{ij}^{\text{bond}} = \begin{cases} c\delta_{i,1}\delta_{j,1} - \frac{\epsilon}{2}\delta_{i,1}\delta_{j,n+1} - \frac{\epsilon}{2}\delta_{i,n+1}\delta_{j,1} + \frac{\epsilon}{2}\delta_{i,n}\delta_{j,n} - \frac{\epsilon}{2}\delta_{i,2n}\delta_{j,2n} & \text{if } \kappa \leq 0, \\ 2c^2\delta_{i,1}\delta_{j,1} - \frac{\epsilon}{2}\delta_{i,1}\delta_{j,n+1} - \frac{\epsilon}{2}\delta_{i,n+1}\delta_{j,1} + \frac{\epsilon}{2}\delta_{i,n}\delta_{j,n} - \frac{\epsilon}{2}\delta_{i,2n}\delta_{j,2n} & \text{if } \kappa > 0. \end{cases} \quad (16)$$

The $N \times N$ matrices (C) , (D) , (V) , and (κ/r) are given by

$$(C)_{ij} = \int B_i(r)B_j(r)dr, \quad (17)$$

$$(D)_{ij} = \int B_i(r)\frac{d}{dr}B_j(r)dr, \quad (18)$$

$$\left(\frac{\kappa}{r}\right)_{ij} = \int B_i(r)\frac{\kappa}{r}B_j(r)dr, \quad (19)$$

$$(V)_{ij} = \int B_i(r)V(r)B_j(r)dr. \quad (20)$$

Equation (13) is known as a generalized eigenvalue problem that can be solved by employing the standard techniques from the linear algebra. In the present work, we have used the well-established Linear Algebra Package 3.3.1 (LAPACK) [52].

C. B-splines

Following the de Boor textbook [53], we divide the interval of interest $[0, R]$ into segments whose endpoints define a knot sequence $\{t_i\} = 1, 2, \dots, N + k$, where R is the cavity radius. The B-splines of the order k , $B_{i,k}(r)$, are defined on this knot sequence by the recurrence relation,

$$B_{i,k}(r) = \frac{r - t_i}{t_{i+k-1} - t_i} B_{i,k-1}(r) + \frac{t_{i+k} - r}{t_{i+k} - t_{i+1}} B_{i+1,k-1}(r), \quad (21)$$

where the B-splines of the first order read as

$$B_{i,1}(r) = \begin{cases} 1, & t_i \leq r \leq t_{i+1} \\ 0, & \text{otherwise} \end{cases}. \quad (22)$$

The first $1, 2 \dots k$ and the last $N + 1, N + 2 \dots N + k$ knots must be equal and are defined as $t_1 = t_2 = \dots = t_k = 0$ and $t_{N+1} = t_{N+2} = \dots = t_{N+k} = R$. Otherwise, the t_i knots with $k < i < n$ follow an exponential grid.

Eigenstates of Eq. (13) labeled by $i = 1, \dots, N$ address the negative continuum $\epsilon_i < -2mc^2$ while solutions with $i = N + 1, \dots, 2N$ describe bound states (the first few ones) and the continuum $\epsilon_i > 0$.

TABLE I. Eigenvalues (a.u.) with $\Pi = 0$ and $J = 0$ for the ground state ($1s^2$) and first two excited states ($1s2s$, $1s3s$) in heliumlike U ($Z = 92$). Values are compared with respective ones listed in Ref. [59].

	E_{1s^2}	E_{1s2s}	E_{1s3s}
This work	-9636	-6081	-5380
Ref. [59]	-9605	-6067	-5369

D. Numerical stability of the CI method

Before providing results for the application of the CI method to the stabilization method it is worthwhile to attest the quality of the obtained states. Following previous works with single-electron spectrum constructed from B-splines (e.g., [54–57]), the spectrum was attested with variations of the B-spline parameters, namely the order (k) and number of splines (N). Optimal values of these parameters are $k = 9$ and $N > 60$, matching with analytical solutions at 13 digits for the first five bound states. This optimization was made for a large enough radius of $R = 40$, in which cavity effects are not present. Through all calculations, these parameters were set constant with the exception of the radius. The effect of finite-nuclear size was found negligible within the quoted precision for all values obtained from the stabilization method presented in Sec. III.

These single-state orbitals were included in the CI matrix (4) for diagonalization. Since the finite-basis method discretizes the continua, spurious autoionizing states can result from this discretization of the negative and positive continua. In detail, this could lead to a sum of discrete negative eigenstates and positive ones in the CI diagonal terms, which could have energies close to two-electron bound states, and thus distort the spectrum. To avoid these spurious autoionizing states, discrete negative states were not included in the CI matrix. Excluding these states is similar to the projection method in the multiconfiguration Dirac-Fock method [58]. For the case of $\Pi = 0$ and $J = 0$ spectra, orbitals of type $nsn's$, $npn'p$, $nsn'd$, and $ndn'd$, with $n \leq 3$ and $n' \leq 10$, were included to form the two-electron wave function (2). Hereafter, we refer to each eigenvalue by the configuration of the dominant CSF, e.g., the ground state with $\Pi = 0$ and $J = 0$ is referred to as $1s^2$. Further increase of these maximum number of orbitals and orbital momentum converge to changes in the six digits. Table I contains the ground state $1s^2$ and first two excited states, i.e., $1s2s$ and $1s3s$ calculated for $Z = 92$, as well as *state-of-the-art* calculations in Ref. [59] that contain full inclusion of Breit interaction and QED effects. The energy values are in agreement with this reference within 0.2%–0.3% relative difference, which is attributed to these extra QED effects.

All obtained eigenvalues for the application of the stabilization method have $\Pi = 0$ and $J = 0$.

III. RESULTS AND DISCUSSIONS

The stabilization diagram constructed with the first 20 energy eigenvalues of the He atom lying between -3.0 a.u. and -0.5 a.u. is given in the upper panel of Fig. 1. The cavity

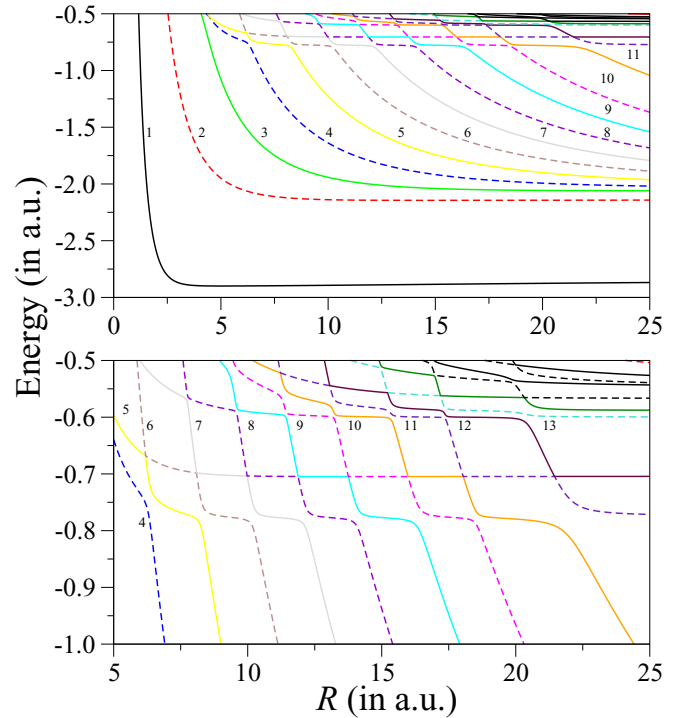


FIG. 1. Stabilization diagram constructed with the energy eigenvalues obtained after solving Eq. (4) with $\Pi = 0$ and $J = 0$ in the function of the cavity radius and for helium atom ($Z = 2$). Configurations of state functions up to $l = 2$ are included in the calculation. Each line (with specific color and style) represents an eigenvalue sorted by energy, e.g., the solid black line represents the first eigenroot, the dashed red line represents the second eigenroot, the solid green line represents the third eigenroot, and so on. Note that the lower panel uses the same color code for the energy eigenroots as that of the upper panel.

radius R is varied in the range 1.0 a.u. to 25.0 a.u. in the mesh size of 0.01 a.u. It is evident from Fig. 1 that the first energy eigenvalue, i.e., the ground state ($1s^2$) is almost insensitive with respect to $R \in [2, 25]$ a.u. Before going into the resonance structure of the system for high R , we analyze the features observed in the strong confinement region. Decrease of R below 2 a.u. causes a drastic effect on the ground-state energy of He. In fact, the curve exhibits a sharp bend, i.e., a “knee” and becomes nearly parallel to the vertical (energy) axis leading to the fragmentation threshold for $R \sim 1.1$ a.u. For the second and the third energy eigenvalues, i.e., the first $1s2s$ and the second $1s3s$ singly excited states of He, such “knee” occurs at larger values of cavity radius (R). The energy eigenvalues of $1sns$ ($n=1-3$) of the He atom, for different values of cavity radius (R) are given in Table II. The present energy values are compared with the benchmark nonrelativistic results of Bhattacharyya *et al.* [60] calculated with the Hylleraas-type basis set. In order to estimate the relativistic contribution, we evaluate these energies with Eqs. (9) and (10) having the full relativistic wave function (large and small components), and without the small component, respectively. We note that the present CI method gives lower values of total energy compared with Ref. [60], as cavity radius decreases. As observed in Table II, this is not due to

TABLE II. First three eigenvalues [$1sns$ ($n = 1-3$)] of the helium atom for several confinement radii R (a.u.) calculated in the present work. E_{L+S} (a.u.) and E_L (a.u.) are the energies calculated with the CI method having the large and small components of the wave functions, and only the large component, respectively. Nonrelativistic results of Bhattacharyya *et al.* [60] are shown for comparison.

R	E_{L+S}	E_L	Ref. [60]
1.11	-0.0988	-0.0991	-0.0739
1.15	-0.4004	-0.4007	-0.3792
1.3	-1.2426	-1.2429	-1.2310
1.5	-1.9116	-1.9118	-1.9070
2	-2.6027	-2.6028	-2.6040
3	-2.8694	-2.8695	-2.8724
4	-2.8973	-2.8974	-2.9005
5	-2.9001	-2.9001	-2.9034
∞	-2.9001	-2.9001	-2.9037
2.31	-0.0339	-0.0341	-0.0283
2.35	-0.1282	-0.1284	-0.1230
2.4	-0.2386	-0.2387	-0.2339
2.5	-0.4369	-0.4371	-0.4332
2.7	-0.7607	-0.7609	-0.7583
3.0	-1.1152	-1.1153	-1.1141
5.0	-1.9494	-1.9494	-1.9497
∞	-2.1402	-2.1401	-2.1459
3.21	-0.0921	-0.0921	-0.0062
3.3	-0.1471	-0.1472	-0.0724
3.5	-0.2507	-0.2507	-0.2016
4	-0.4562	-0.4563	-0.4582
5	-1.0796	-1.0797	-1.0792
∞	-2.0595	-2.0595	-2.0613

the inclusion of relativity since an estimation of these effects based on the small component returns a negligible influence. These differences between relativistic and nonrelativistic values are slightly amplified on lower values of R where the total energies are more sensitive to this parameter. A closer look to the CI matrix (4) at $R = 1.11$ a.u. and to the first two diagonal terms ($1s^2$ and $1s2s$) shows that the orbital energies $2\epsilon_{1s}$ are set apart from $\epsilon_{1s} + \epsilon_{2s}$ by ~ 10 a.u., while Coulomb repulsion between these states equals $V_{1s^2,1s2s} = 0.6$ a.u.. This makes the $1s^2$ state less influenced by mixing of the $1s2s$ state, as well as by the rest of the spectrum. As consequence, the value of the $1s^2$ state at $R = 1.11$ is mainly given by $2\epsilon_{1s} + V_{1s^2,1s^2}$. Further verification from the Hylleraas method can thus be traced back to these terms. The atomic electrons cease to be in a bound state if the cavity radius decreases below a critical value, denoted as R_c . In case of the $1s^2$ state this occurs when the orbital energies (ϵ_{1s}) match the Coulomb repulsion energy ($V_{1s^2,1s^2}$). The critical cavity radii (R_c) corrected up to two decimal place for $1s^2$, $1s2s$, and $1s3s$ states are estimated as 1.10 a.u., 2.30 a.u., and 3.08 a.u., respectively. The bound electron(s) will detach from the atom if $R < R_c$ and the cavity-bound free electron continuum becomes discrete. But still the electrons in the continuum remain bound by the cavity and entangled to the parent ion [61]. We have also calculated these quantized positive energy states of the electrons in the presence of the ion in the center of the confining sphere. For $R = 1.0$ a.u., energy of the ground state of the cavity bound

atom is 0.9769 a.u., the first excited state is 13.8676 a.u., and the second excited state is 14.3220 a.u. Further reduction of R to 0.5 a.u. yields these values at 22.2728 a.u., 67.3502 a.u., and 68.4632 a.u., respectively. The present results are in reasonable agreement with the nonrelativistic results [61,62] estimated in the correlated Hylleraas basis.

Under an adiabatic approximation, the amount of pressure (P) “felt” by the system inside the impenetrable cavity can be expressed as

$$P = -\frac{1}{4\pi R^2} \frac{dE_g}{dR} \simeq -\frac{1}{4\pi R^2} \frac{\Delta E_g}{\Delta R}, \quad (23)$$

where E_g is the ground-state energy of the system inside the sphere of radius R . For higher excited states, this relation may not be applicable as the equilibrium criteria is not satisfied because of finite lifetimes of such states. However, we can assume that the amount of pressure experienced by the ion would be the same for all the states at a particular value of R . Therefore, the pressure (P) at a particular value of R felt by an ion in an excited state can be estimated from Eq. (23) by calculating the energy gradient of the ground state $1s^2$ with respect to R around the same value of R . In the present calculation, we have taken $\Delta R = 10^{-4}$ a.u. The critical pressure (P_c) or the ionization pressure, i.e., the pressure experienced by the He atom at the critical cavity radius (R_c) values 1.10 a.u., 2.30 a.u., and 3.08 a.u. are estimated as 1611 GPa, 150.4 GPa, and 14.4 GPa, respectively. These P_c values are in excellent agreement with that of Saha *et al.* [63] and establishes the applicability of the present method in strong confinement region.

The upper panel of Fig. 1 reveals that all the higher energy eigenvalues vary significantly with respect to cavity radius (R) and produces a flat, short plateau in the vicinity of the avoided crossing. Enlarged view of such avoided crossings within the energy range from -1.0 to -0.5 a.u. is given in the lower panel of Fig. 1. It clearly appears that such plateaus occur at some particular energy values that are the positions of the resonances. For instance, it can be observed that the first resonance position is close to -0.77 a.u. Precise determination of the resonance parameters, i.e., positions and widths of these states are done in a two-step process. The first step is to take an eigenvalue (single color line in Fig. 1) and estimate the spectral density of states (DOS) from the stabilization diagram by taking the inverse of tangent at different points near the stabilization plateau for each energy eigenvalue using the formula:

$$\rho_n(E) = \left| \frac{R_{i+1} - R_{i-1}}{E_n(R_{i+1}) - E_n(R_{i-1})} \right|. \quad (24)$$

For a clear visualization, the eighth energy eigenvalue showing the plateau near -0.77 a.u. and corresponding spectral DOS are plotted within the energy range $-0.81 \leq E \leq -0.74$ a.u. in Fig. 2. The DOS plot shows a peak in the middle of the plateau [follow the dashed red line showing the position of the lowest lying ($2s^2$) resonance below $\text{He}^+(2s)$].

As one eigenvalue may produce plateaus at different energies (see Fig. 1), corresponding peaks of DOS will occur at those values. The DOS profiles of eigenvalues 5–10 within the range $-0.85 \leq E \leq -0.50$ a.u. are given explicitly in Fig. 3. It is clear that three peaks at three different energies

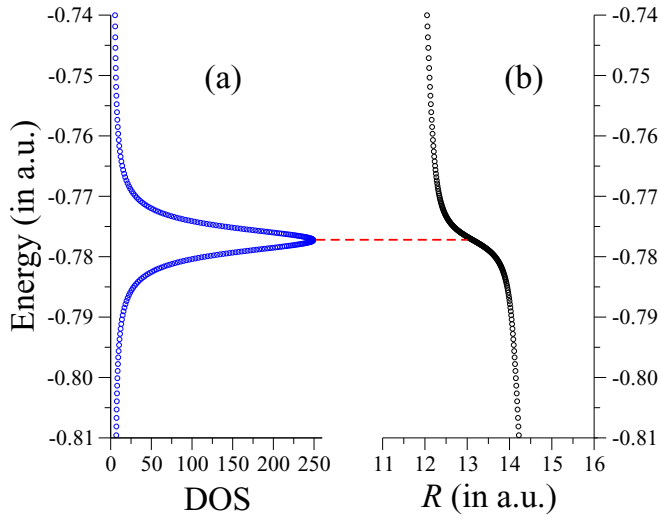


FIG. 2. Combined plot of numerically estimated DOS [Eq. (24)] vs energy (in a.u.) for eigenvalue No. 8 from the stabilization diagram of Fig. 1.

are converging for first three resonances. Among these three DOS peaks, the middle one near -0.7 a.u. represents a very narrow width, evident from the plots eigenvalues 8–10. Thus the lifetime of this state is considerably high compared to the other two states lying on either sides. This state corresponds to $2p^2$. The next peak around -0.59 a.u. is the $2s3s$ state while the first peak around -0.77 a.u. corresponds to the $2s^2$

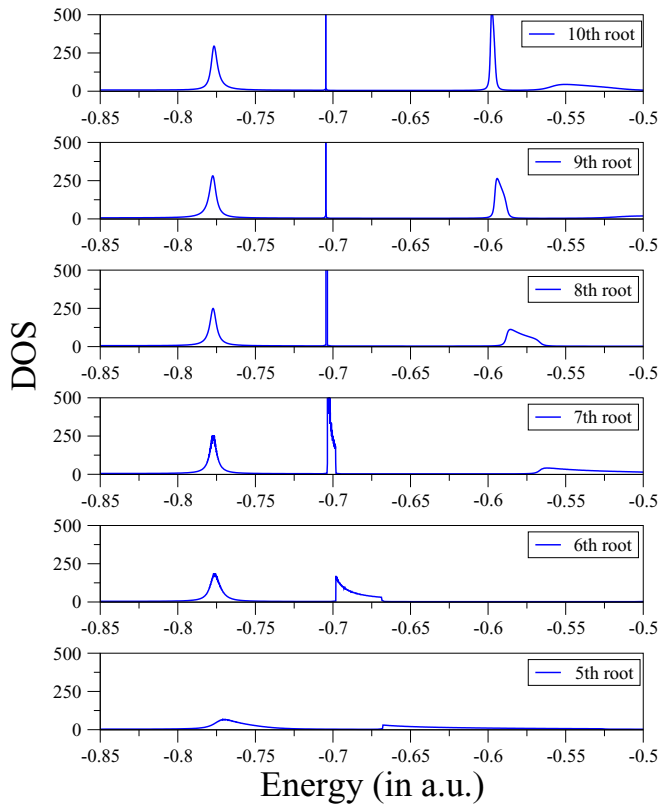


FIG. 3. The DOS peaks of eigenvalue Nos. 5–10 in the energy range -0.85 a.u. to -0.50 a.u.

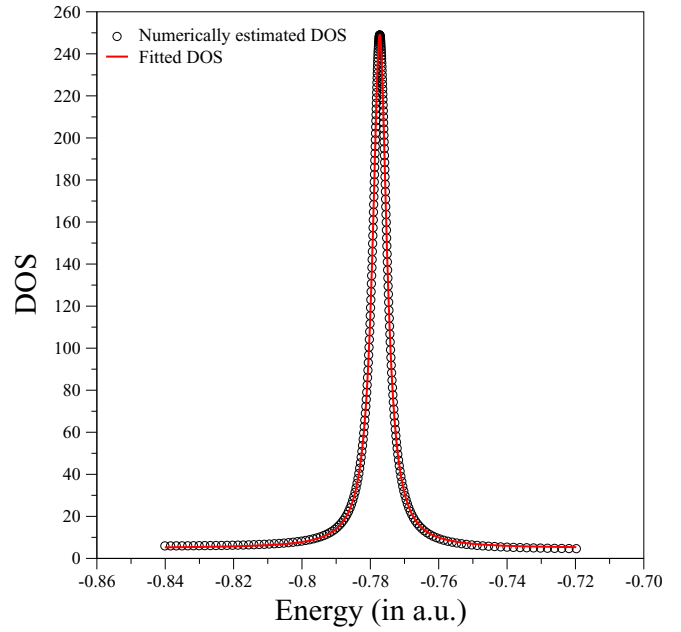


FIG. 4. Numerically estimated DOS vs energy (in a.u.) (black hollow circles) and the fitted Lorentzian (solid red line) for eigenvalue No. 8 showing the first resonance (~ -0.77 a.u.) of He below the $\text{He}^+(2s)$ threshold.

state. It is also evident that these resonances are isolated as the separation of peaks are greater than the widths of the consecutive resonances.

In the next step, we consider DOS of each isolated resonance and fit it with a Lorentzian profile,

$$\rho_n(E) = y_0 + \frac{A}{\pi} \frac{\Gamma/2}{(E - E_r)^2 + (\Gamma/2)^2}, \quad (25)$$

where Γ is the full width at half maximum of the peak, y_0 is the offset, A represents the area under the curve from the base line, and E_r is the energy corresponding to maximum of ρ_n , i.e., the resonance position. As an example, the estimated DOS and the fitted Lorentzian corresponding to eigenvalue No. 8 is given in Fig. 4. The fitting to this curve [Eq. (25)] yields the resonance parameters $E_r = -0.77726$ a.u. and $\Gamma = 0.00502$ a.u. ($\chi^2 = 0.09964$, $\mathcal{R}^2 = 0.99999$). This is the lowest lying 1S_0 resonance below $\text{He}^+(2s)$. Repeated calculations of DOS near the plateau of each of the eigenvalues for the resonance states are performed, which result in fitted Lorentzian similar to Fig. 4. For a particular resonance, the position and width is chosen with respect to the best fitting parameters. For instance, among the fitting parameters (χ^2 , \mathcal{R}^2) of the first DOS peak of eigenvalues 8–10, we find eigenvalue No. 8 yields the least χ^2 value and also \mathcal{R}^2 value closer to unity. Similar fitting for the second resonance yields $E_r = -0.70466$ a.u., $\Gamma = 0.0000368$ a.u. while for the third resonance, we find $E_r = -0.59731$ a.u., $\Gamma = 0.0031956$ a.u. The resonance parameters (E_r , Γ) for other states can be obtained in a similar manner. The estimated resonance parameters of the first and third resonances of He atom are in good agreement with the benchmark nonrelativistic numerical records [46,47] for resonances below the second ionization threshold of the He atom. For instance, Abrashkevich *et al.* [46] reported

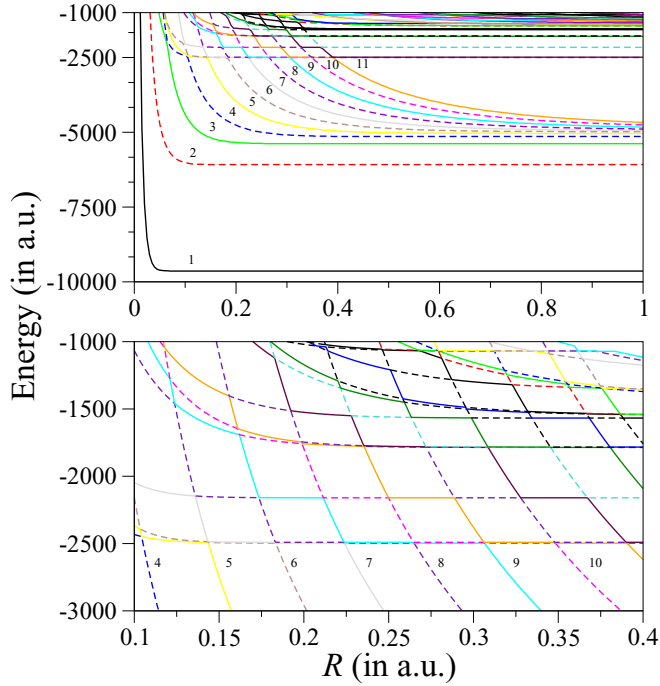


FIG. 5. Stabilization diagram constructed with the energy eigenvalues obtained after solving Eq. (4) with $\Pi = 0$ and $J = 0$ in the function of the cavity radius and for the heliumlike uranium atom ($Z = 92$). Configurations of state functions up to $l = 2$ are included in the calculation. Each line represents an eigenvalue sorted by energy. Each line (with specific color and style) represents an eigenvalue sorted by energy, e.g., solid black line represents the first eigenroot, dashed red line represents the second eigenroot, solid green line represents the third eigenroot, and so on. Note that the lower panel uses the same color code for the energy eigenroots as that of the upper panel.

the resonance positions of the first and third resonances as -0.778824 a.u. and -0.590158 a.u., respectively, by adopting coupled-channel hyperspherical adiabatic approach. Explicitly the correlated Hylleraas-type basis set in the framework of complex-coordinate-rotation calculation of Burgers *et al.* [47] yields the highly precise estimate of widths of first and third resonances as 0.004541126 a.u. and 0.001362478 a.u., respectively.

After standardizing the stabilization method within the relativistic CI framework for the He atom, we extend it to determine the resonance structure of highly charged heliumlike uranium ($Z = 92$) where relativistic effects play a major role. The stabilization diagram of $\Pi = 0$ and $J = 0$ states of U^{90+} is given in Fig. 5. In the upper panel, the diagram displays the first 20 energy eigenvalues within the range from -10000.0 a.u. to -1000 a.u. The ground ($1s^2$) and first two excited states, i.e., $1s2s$ and $1s3s$, respectively (energies listed in Table I), lying below the $U^{91+}(1s)$ threshold, are evident from Fig. 5. In the strong confinement regime, these states show the same pattern as of He (Fig. 1) except the positions of the respective “knees,” which occur at lower values of R as compared to He, due to the contraction of the wave functions in the much stronger Coulomb field.

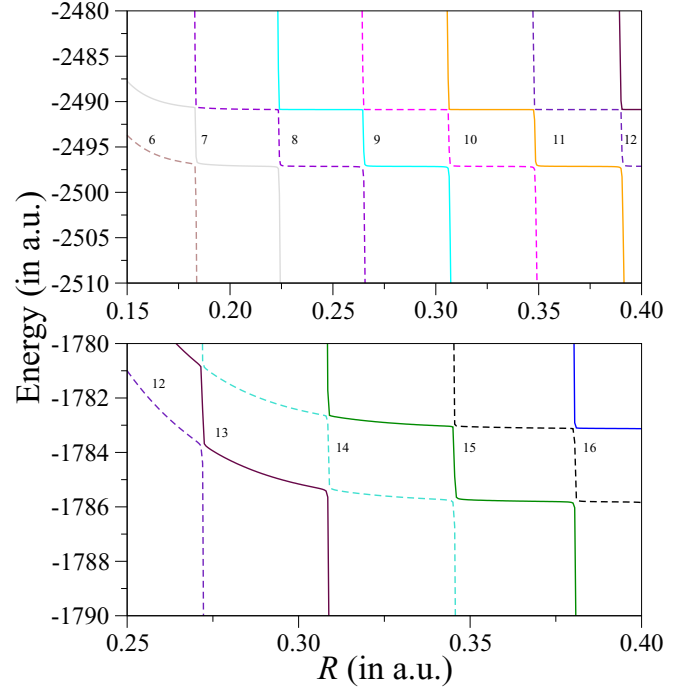


FIG. 6. Enlarged view of the stabilization diagram given in Fig. 5. For both upper and lower panels, the line colors and styles carry similar meaning as Fig. 5.

An enlarged view of the stabilization diagram of U^{90+} in the energy range -3000 a.u. to -1000 a.u. is given in the lower panel of Fig. 5. The energy range is properly chosen to locate the resonances between $1s$ and $2s$ thresholds of U^{91+} . A series of resonances of heliumlike uranium near the energies -2495 a.u., -2159 a.u., -1783 a.u., -1556 a.u. are seen. A closer look at the avoided crossings of the eigenvalues near the energies -2495 a.u. and -1783 a.u. are shown in the upper and lower panels of Fig. 6, respectively. A pair of close resonances at $(-2497.12$ a.u., -2490.87 a.u.) in the upper panel and $(-1785.57$ a.u., -1783.04 a.u.) in the lower panel are visible in Fig. 6. As the pair of resonances are very closely spaced, we have taken a much lesser mesh size (0.0001 a.u.) of R compared to that taken for He for the precise determination of the DOS profiles. Figures 7 and 8 display plot of the numerically estimated DOS vs energy (in a.u.) for eigenvalue No. 11 showing close lying first and second resonances, respectively, of heliumlike uranium below the $U^{91+}(2s)$ threshold. The fitting to the curve given in Fig. 7 yields $E_r = -2497.1405$ a.u. and $\Gamma = 0.01682$ a.u. ($\chi^2 = 0.000003$, $\mathcal{R}^2 = 0.99999$) while the same in Fig. 8 yields $E_r = -2490.87841$ a.u. and $\Gamma = 0.00126$ a.u. ($\chi^2 = 0.01625$, $\mathcal{R}^2 = 0.99998$). The fitting further confirms that the pair of resonances are isolated despite being closely spaced. In a similar fashion using eigenvalue No. 12, we have determined $E_r = -2159.9825$ a.u. and $\Gamma = 0.00096$ a.u. for the third resonance and the corresponding plot is given in Fig. 9. The parameters of the first six resonance states of heliumlike uranium are depicted in Table III. Sharp gradual decrement of the width of the resonance states are noticed which may be due to respective increase in the interelectronic separation. It is to be noted that only the tentative positions are reported for the fourth, fifth, and sixth

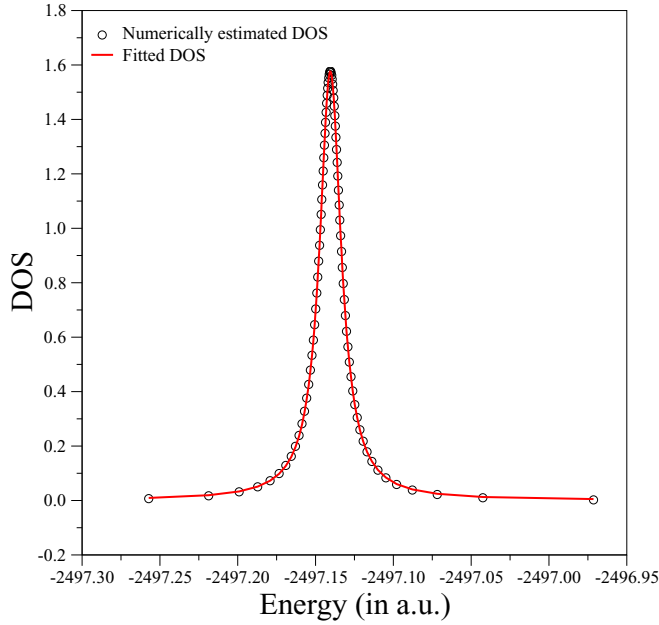


FIG. 7. Numerically estimated DOS vs. Energy (in a.u.) (black hollow circles) and the fitted Lorentzian (solid red line) for eigenvalue no. 11 showing 1st resonance (~ -2497 a.u.) of heliumlike uranium below $U^{91+}(2s)$ threshold.

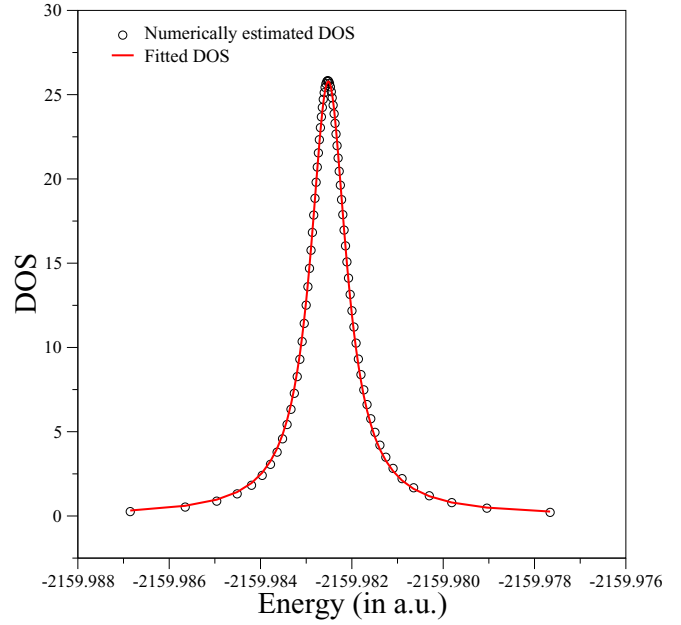


FIG. 9. Numerically estimated DOS vs energy (in a.u.) (black hollow circles) and the fitted Lorentzian (solid red line) for eigenvalue No. 12 showing third resonance (~ -2159 a.u.) of heliumlike uranium below $U^{91+}(2s)$ threshold.

resonances. Accurate determination of width of these states are in the pipeline with more configurations in the basis set. To the best of our knowledge, this is the first prediction of the parameters of low-lying resonances of heliumlike uranium ion and therefore warrants precise experimental verification.

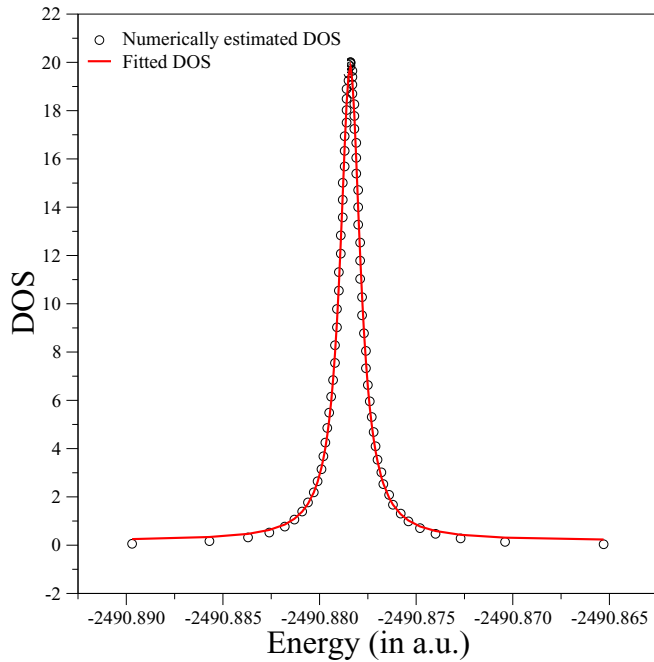


FIG. 8. Numerically estimated DOS vs energy (in a.u.) (black hollow circles) and the fitted Lorentzian (solid red line) for eigenvalue No. 11 showing second resonance (~ -2490 a.u.) of heliumlike uranium below $U^{91+}(2s)$ threshold.

The present results with $Z = 2$ and 92 establishes the applicability of the relativistic configuration-interaction (CI) framework to the stabilization method for any two-electron system. More CSFs ($l > 2$) in the present framework will certainly increase the possibility of locating more number of resonances below the threshold. It would also be interesting to see the effect of QED on the parameters of these resonances in future. In order to construct the resonance wave function, we can choose the R value for an appropriate eigenvalue at which the DOS reaches its maximum. However, in case of very narrow resonances, the R value at the midpoint of the plateau of a particular eigenvalue can fairly be chosen. Having the idea of the resonance wave function more structural information about the state may be extracted.

This method is applicable to any total angular momentum state ($^{2s+1}L_J$) of heliumlike ions and in principle to the complex resonance structures of many-electron systems. It can also be used to study the behavior of bound states of few-electron ions inside a finite domain to realize the pressure confinement. As an example, we choose a two-electron

TABLE III. Parameters of first six resonance states of heliumlike U ($Z = 92$) below $U^{91+}(2s)$ threshold.

State	Resonance energy E_r (a.u.)	Resonance width Γ (a.u.)
1	-2497.1405	0.01682
2	-2490.8784	0.00126
3	-2159.9825	0.00096
4	~ -1785.81	—
5	~ -1783.11	—
6	~ -1567.75	—

ion embedded in dense plasma environment belonging to strong coupling regime considering the ion-sphere (IS) model potential [64] where the two-body interaction between the nucleus and a bound electron is given by

$$V_{\text{IS}}(r_i) = -\frac{Z}{r_i} + \frac{Z - N_e}{2R} \left[3 - \left(\frac{r_i}{R} \right)^2 \right]. \quad (26)$$

Here Z is the nuclear charge of the positive ion and N_e is the number of bound electrons. R is the IS radius which is determined from the charge neutrality condition,

$$Z - N_e = \frac{4}{3}\pi R^3 n_e. \quad (27)$$

The density of plasma electrons (n_e) thus governs the size of the sphere (Wigner-Seitz sphere) [64]. Due to the spatial finiteness of the IS potential, the wave function of the bound electrons is truncated at the boundary of the Wigner-Seitz sphere. Considering the experimental interest in the dense aluminum plasma [65], we have made an attempt to estimate the ground-state energy of the heliumlike aluminum ion as a test case. It has been found that the present method yields ground-state energy eigenvalues -156.653 a.u., -151.299 a.u., and -148.682 a.u. for $n_e = 5 \times 10^{22}$ per cm^3 , 5×10^{23} per cm^3 , and 1×10^{24} per cm^3 , respectively. The present values are in reasonable agreement with those estimated by Chen *et al.* [66] using multiconfiguration Dirac-Fock (MCDF) wave functions with the inclusion of a finite nuclear size and QED corrections.

IV. CONCLUSION

The stabilization method in the relativistic configuration-interaction framework has been adopted to investigate the isolated resonances of He and heliumlike uranium ion with $\Pi = 0$ and $J = 0$. The ions are considered to be enclosed within an impenetrable spherical cavity, the radius of which is varied continuously. The stabilization diagram is therefore realized with respect to the radius of the cavity (R). The advantage of this diagram is that one can obtain the tentative positions of all the resonances admissible for a given basis size. It has been noted that a single eigenroot of the diagonalized Hamiltonian may form a flat plateau in the vicinity of avoided crossings at several resonance energies. Therefore, different roots show flat plateau in the vicinity of avoided crossings for particular resonance energy. The DOS profiles are used to determine the parameters of the resonance states. In case of isolated resonances, the DOS is numerically estimated by taking the inverse of tangent at different points near the flat plateaus which are expected to fit with perfect Lorentzian functions. But the shape of the numerically estimated DOS profile depends on two major factors: First the

quality and size of the basis set which actually determines whether a resonance is properly localized by a particular eigenroot of the diagonalized Hamiltonian or not. Therefore, a distorted DOS profile for a particular root implies that the root does not adequately represent the given resonance. We have shown the dependence of the DOS profiles corresponding to different resonances on the diagonalized eigenroots. Nevertheless, we can choose the best fitted DOS profile (looking at the statistical fitting parameters χ^2 and \mathcal{R}^2) from different roots to estimate the position and width of a particular isolated resonance. The second important factor is the mesh size of the basis set and stabilizing parameters (here in the present work, it is the radial extent of the wave function R). Due to obvious reasons, the accuracy of the numerical value of DOS at different energy positions in the neighbourhood of the plateau is quite sensitive on the mesh size. The lesser the mesh size, the variation of tangent at different points in the plateau region will be more accurate. For narrow resonance or in the case of two closely spaced isolated resonances (not necessarily narrow), the numerical errors can essentially be avoided by considering lesser mesh size of R . We have determined the parameters of two closely spaced resonances of heliumlike uranium accurately just by increasing the mesh size. In summary, there is always a scope of improving the accuracy of the DOS profiles and therefore the precision of the estimated resonance parameters by increasing the number of terms in the basis set (or the radial extension of the basis set) as well as by decreasing the mesh size of the stabilizing parameter. In the strong confinement regions, we have also determined the variation of the bound state energies with respect to the cavity radius (R) and made an estimate about the pressure felt by the atom inside the cavity. Moreover, we have shown how the present method can be useful to determine the bound state energies of highly charged ions in the strongly coupled plasma environment. This hybrid technique has the potential to enable investigating the resonance structures of highly charged ions of high- Z elements.

ACKNOWLEDGMENTS

This research was supported in part by Fundação para a Ciência e a Tecnologia (FCT), Portugal, through the research center Grants No. UID/FIS/04559/2019 and No. UID/FIS/04559/2020 (LIBPhys), from FCT/MCTES/PIDDAC, Portugal. P.A. acknowledges support from the FCT, under Contract No. SFRH/BPD/92329/2013. J.K.S. acknowledges partial financial support from the DHESTBT, Government of West Bengal, under Grant No. 249(Sanc.)/ST/P/S & T/16G-26/2017. S.B. acknowledges financial assistance through Grant No. 23(Sanc.)/ST/P/S & T/16G-35/2017 from DHESTBT, Government of West Bengal, India.

-
- [1] B. Rudek, S.-K. Son, L. Foucar, S. W. Epp, B. Erk, R. Hartmann, M. Adolph, R. Andritschke, A. Aquila, N. Berrah *et al.*, *Nat. Photon.* **6**, 858 (2012).
 [2] T. Katravulapally and L. A. A. Nikolopoulos, *Atoms* **8**, 35 (2020).
 [3] S. Barmaki, M. A. Albert, and S. Laulan, *Phys. Scr.* **95**, 055403 (2020).
 [4] S. Dutta, A. N. Sil, J. K. Saha, and T. K. Mukherjee, *Int. J. Quantum Chem.* **119**, e25981 (2019).
 [5] M. Nrisimhamurty, G. Aravind, P. C. Deshmukh, and S. T. Manson, *Phys. Rev. A* **91**, 013404 (2015).
 [6] Y. K. Ho, *Phys. Rep.* **99**, 1 (1983).
 [7] B. I. Schneider, *J. Phys.: Conf. Ser.* **759**, 012002 (2016).
 [8] A. U. Hazi and H. S. Taylor, *Phys. Rev. A* **1**, 1109 (1970).

- [9] M. F. Fels and A. U. Hazi, *Phys. Rev. A* **4**, 662 (1971).
- [10] V. A. Mandelshtam, T. R. Ravuri, and H. S. Taylor, *Phys. Rev. Lett.* **70**, 1932 (1993).
- [11] E. A. Hylleraas and B. Undheim, *Z. Phys.* **65**, 759 (1930).
- [12] J. K. L. MacDonald, *Phys. Rev.* **43**, 830 (1933).
- [13] R. J. Drachman and S. K. Houston, *Phys. Rev. A* **14**, 894 (1976).
- [14] Y. K. Ho, *Phys. Rev. A* **19**, 2347 (1979).
- [15] J. Müller, X. Yang, and J. Burgdörfer, *Phys. Rev. A* **49**, 2470 (1994).
- [16] S. Kar and Y. K. Ho, *Phys. Rev. E* **70**, 066411 (2004).
- [17] S. Kar and Y. K. Ho, *Phys. Rev. A* **71**, 052503 (2005).
- [18] S. Kar and Y. K. Ho, *Phys. Rev. A* **72**, 010703(R) (2005).
- [19] S. Kar and Y. K. Ho, *J. Phys. B: At. Mol. Opt. Phys.* **39**, 2445 (2006).
- [20] S. Kar and Y. K. Ho, *Phys. Rev. A* **75**, 062509 (2007).
- [21] A. Ghoshal and Y. K. Ho, *Phys. Rev. A* **79**, 062514 (2009).
- [22] J. K. Saha and T. K. Mukherjee, *Phys. Rev. A* **80**, 022513 (2009).
- [23] J. K. Saha, S. Bhattacharyya, and T. K. Mukherjee, *J. Chem. Phys.* **132**, 134107 (2010).
- [24] J. K. Saha, S. Bhattacharyya, T. K. Mukherjee, and P. K. Mukherjee, *Int. J. Quantum Chem.* **111**, 1819 (2011).
- [25] S. Kasthurirangan, J. K. Saha, A. N. Agnihotri, S. Bhattacharyya, D. Misra, A. Kumar, P. K. Mukherjee, J. P. Santos, A. M. Costa, P. Indelicato, T. K. Mukherjee, and L. C. Tribedi, *Phys. Rev. Lett.* **111**, 243201 (2013).
- [26] J. K. Saha, S. Bhattacharyya, and T. K. Mukherjee, *Commun. Theor. Phys.* **65**, 347 (2016).
- [27] A. Sadhukhan, S. Dutta, and J. K. Saha, *Eur. Phys. J. D* **73**, 250 (2019).
- [28] S. A. Deutscher, X. Yang, and J. Burgdörfer, *Nucl. Instrum. Methods Phys. Res. Sect. B* **100**, 336 (1995).
- [29] A. Landau and I. Haritan, *J. Phys. Chem. A* **123**, 5091 (2019).
- [30] T. González-Lezana, G. Delgado-Barrio, P. Villarreal, and F. X. Gadéa, *Eur. Phys. J. D* **20**, 227 (2002).
- [31] M. A. Fennimore and S. Matsika, *Phys. Chem. Chem. Phys.* **18**, 30536 (2016).
- [32] M. A. Fennimore and S. Matsika, *J. Phys. Chem. A* **122**, 4048 (2018).
- [33] L. Zhang, S.-G. Zhou, J. Meng, and E.-G. Zhao, *Phys. Rev. C* **77**, 014312 (2008).
- [34] D. Salzmann, *Atomic Physics in Hot Plasmas* (Oxford University Press, Oxford, 1998).
- [35] V. Dolmatov, A. Baltenkov, J.-P. Connerade, and S. Manson, *Radiat. Phys. Chem.* **70**, 417 (2004).
- [36] Z.-Y. Deng, J.-K. Guo, and T.-R. Lai, *Phys. Rev. B* **50**, 5736 (1994).
- [37] J. L. Movilla and J. Planelles, *Phys. Rev. B* **71**, 075319 (2005).
- [38] L. Zhou, Y. Xing, and Z. P. Wang, *Eur. Phys. J. B* **85**, 212 (2012).
- [39] L. F. Pašteka, T. Helgaker, T. Saue, D. Sundholm, H.-J. Werner, M. Hasanbulli, J. Major, and P. Schwerdtfeger, *Mol. Phys.* **118**, e1730989 (2020).
- [40] J.-P. Connerade, *J. Alloys Compd.* **255**, 79 (1997).
- [41] S. Bhattacharyya, J. K. Saha, and T. K. Mukherjee, *Phys. Rev. A* **91**, 042515 (2015).
- [42] W. Jaskólski, *Phys. Rep.* **271**, 1 (1996).
- [43] E. B. E. John Sabin, *Advances in Quantum Chemistry* (Academic Press, Cambridge, 2009).
- [44] *Electronic Structure of Quantum Confined Atoms and Molecules*, edited by K. D. Sen (Springer International Publishing, Cham, 2014).
- [45] C. H. Maier, L. S. Cederbaum, and W. Domcke, *J. Phys. B: At. Mol. Phys.* **13**, L119 (1980).
- [46] A. G. Abrashkevich, D. G. Abrashkevich, M. S. Kaschiev, I. V. Puzynin, and S. I. Vinitzky, *Phys. Rev. A* **45**, 5274 (1992).
- [47] A. Burgers, D. Wintgen, and J. M. Rest, *J. Phys. B: At. Mol. Opt. Phys.* **28**, 3163 (1995).
- [48] W. R. Johnson, *Atomic Structure Theory: Lectures on Atomic Physics* (Springer, New York, 2007).
- [49] W. R. Johnson, S. A. Blundell, and J. Sapirstein, *Phys. Rev. A* **37**, 307 (1988).
- [50] A. Chodos, R. L. Jaffe, K. Johnson, C. B. Thorn, and V. W. Weisskopf, *Phys. Rev. D* **9**, 3471 (1974).
- [51] W. Greiner, *Theoretical Physics 3* (Springer-Verlag, Berlin, 1990), Vol. 3.
- [52] E. Anderson, Z. Bai, C. Bischof, S. Blackford, J. Demmel, J. Dongarra, J. D. Croz, A. Greenbaum, S. Hammarling, A. McKenney, and D. Sorensen, *LAPACK Users' Guide* (SIAM, Philadelphia, 1999).
- [53] C. de Boor, *Applied Mathematical Sciences* (Springer-Verlag, New York, 1978), Vol. 27.
- [54] J. P. Santos, F. Parente, and P. Indelicato, *Eur. Phys. J. D* **3**, 43 (1998).
- [55] P. Amaro, J. P. Santos, F. Parente, A. Surzhykov, and P. Indelicato, *Phys. Rev. A* **79**, 062504 (2009).
- [56] L. Safari, P. Amaro, S. Fritzsche, J. P. Santos, and F. Fratini, *Phys. Rev. A* **85**, 043406 (2012).
- [57] P. Amaro, F. Fratini, L. Safari, J. Machado, M. Guerra, P. Indelicato, and J. P. Santos, *Phys. Rev. A* **93**, 032502 (2016).
- [58] P. Indelicato, *Phys. Rev. A* **51**, 1132 (1995).
- [59] V. A. Yerokhin and A. Surzhykov, *J. Phys. Chem. Ref. Data* **48**, 033104 (2019).
- [60] S. Bhattacharyya, J. K. Saha, P. K. Mukherjee, and T. K. Mukherjee, *Phys. Scr.* **87**, 065305 (2013).
- [61] P. Kościk and J. K. Saha, *Eur. Phys. J. D* **69**, 250 (2015).
- [62] A. Flores-Riveros, N. Aquino, and H. Montgomery, *Phys. Lett. A* **374**, 1246 (2010).
- [63] J. K. Saha, S. Bhattacharyya, and T. K. Mukherjee, *Int. J. Quantum Chem.* **116**, 1802 (2016).
- [64] S. Ichimaru, *Rev. Mod. Phys.* **54**, 1017 (1982).
- [65] S. M. Vinko, O. Ciricosta, T. R. Preston, D. S. Rackstraw, C. R. D. Brown, T. Burian, J. Chalupský, B. I. Cho, H.-K. Chung, K. Engelhorn, R. W. Falcone, R. Fiokovini, V. Hájková, P. A. Heimann, L. Juha, H. J. Lee, R. W. Lee, M. Messerschmidt, B. Nagler, W. Schlott, J. J. Turner, L. Vysin, U. Zastrau, and J. S. Wark, *Nat. Commun.* **6**, 6397 (2015).
- [66] Z.-B. Chen, K. Ma, Y.-L. Ma, and K. Wang, *Phys. Plasmas* **26**, 082101 (2019).